Materials Transactions, Vol. 62, No. 2 (2021) pp. 205 to 212

Thermal Fatigue Life Prediction of BGA Solder Joints Using a Creep Constitutive Equation Incorporating Microstructural Coarsening Effect

Kouichi Morooka[1,*] and Yoshiharu Kariya[2,*]

[1]*Graduate School of Shibaura Institute of Technology, Tokyo 135-8548, Japan*
[2]*Department of Materials Science and Engineering, Shibaura Institute of Technology, Tokyo 135-8548, Japan*

A thermal fatigue life prediction method is proposed for Sn–Ag–Cu solder joints that incorporates the effect of creep strength reduction due to microstructural coarsening of the solder during thermal cycling. The proposed method was used to predict the thermal fatigue life of solder joints in a BGA (ball grid array) semiconductor package. In the study, the thermal fatigue life was calculated through as follows. A creep constitutive equation for the solder that incorporates the strain-enhanced growth of the intermetallic compounds in the solder was used to update the constitutive equation at each given cycle and the relationship between inelastic strain energy density range and the number of cycles of the solder joint was obtained to calculate the fatigue life. As the number of thermal cycles increased, the intermetallic compounds grew, and in conjunction with this, the inelastic strain energy density range increased, causing the thermal fatigue life of the solder joint to decrease compared with that without the microstructural coarsening effect. Since the growth of intermetallic compounds under field conditions with a long dwell time is large compared with that during accelerated tests, the decrease in thermal fatigue life due to microstructural coarsening was found to be significant under field conditions with a long dwell time. [doi:10.2320/matertrans.MT-M2020313]

(Received October 1, 2020; Accepted November 11, 2020; Published January 12, 2021)

Keywords: *thermal fatigue life prediction, BGA solder joint, microstructural coarsening, creep, finite element method*

1. Introduction

Recently, the number of semiconductors packages used in vehicles and social infrastructure has been greatly increasing. In this situation, long-term reliability of the semiconductor packages is a critical challenge. Since thermal fatigue of solder joints is the key to overcoming the reliability of semiconductor packages, much research has been conducted on prediction of thermal fatigue life. Several approaches have been used for the prediction models for the fatigue life prediction method: the inelastic-strain-range approach, the creep damage approach, and the strain energy density range approach.[1,2] In all these approaches, a constitutive equation is required for calculating the inelastic deformation of the solder by the finite element method (FEM). In general, the constitutive equation derived from material test results of a certain microstructure is used. However, since microstructural coarsening attributable to thermal and strain loads occurs while the semiconductor package is in operation,[3,4] microstructural changes in the constitutive equation need to be incorporated into reliability design. Creep in particular, which controls deformation of solder, is strongly dependent on microstructure, so microstructural coarsening during long-term use leads to a decrease in creep strength.[5] Since the increase in creep deformation causes acceleration of fatigue damage,[6] microstructural changes need to be incorporated in the prediction of thermal fatigue life of the solder joint. Although the use of computer-aided engineering in designing reliability of electronics devices has been progressing recently, the current approach to the thermal fatigue prediction of solder joints is not at the stage where microstructural changes of solder alloys are reflected in the prediction.[2] This study focused on the decrease in creep strength in solder joints due to microstructural coarsening and investigated thermal fatigue predictions of solder joints in BGA (ball grid array) packages in the environment of long-term use.

*Corresponding authors, E-mail: MB19042@shibaura-it.ac.jp, y_kariya@shibaura-it.ac.jp

2. Procedure

2.1 Overview of the thermal fatigue life calculation method

The following procedure was used to calculate the thermal fatigue life of solder joints in a BGA package by incorporating the decrease in creep strength due to microstructural coarsening of the solder alloy.

First, a low cycle test was conducted using a miniature solder joint specimen that mimics the real BGA solder joint in the package. Morrow's law for fatigue life prediction using the inelastic strain energy density range Win was then set up. Since life prediction by Morrow's law is relatively insensitive to microstructure, it was assumed that the life prediction law is not dependent on the microstructure of solder. However, microstructural dependence is taken into account since the creep constitutive equation is sensitive to microstructure. Sn–Ag–Cu alloys are dispersion-strengthened alloys, and their creep strength is assumed to be controlled by the particle size of intermetallic compounds. The growth of the particles is described by the strain-enhanced growth model, which is then incorporated into the creep constitutive equation. The creep constitutive equation is updated at each given cycle to perform thermal stress analysis of the BGA package by FEM. Through these processes, changes in Win associated with the progress of cycling are obtained. This relationship is substituted into the fatigue life prediction law to calculate the thermal fatigue life.

The white frame in Fig. 1 shows the BGA package that was analyzed. The BGA package is composed of a mold resin, FR-4, Si, solder, and copper wiring layers. The solder bumps consist of Sn–3.0 mass%Ag–0.5 mass%Cu (hereinafter, mass% is omitted). The microstructure of the solder

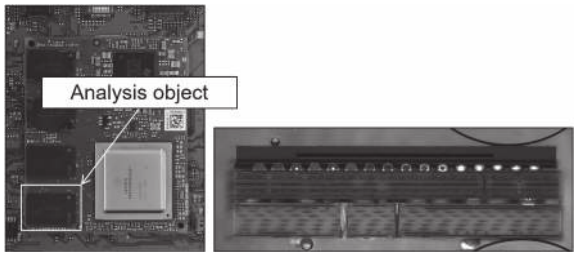

Fig. 1 Photographs of BGA semiconductor package used in this study.

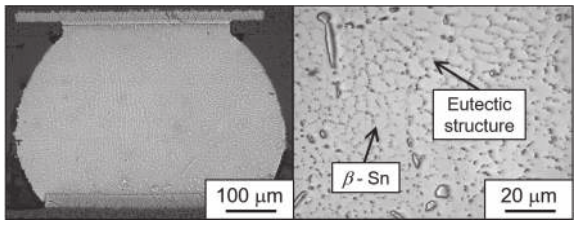

Fig. 2 Optical micrographs of solder bump.

Table 1 Dimensions of BGA semiconductor package.

	Specification / mm
Solder bump pitch	0.8
Solder bump diameter	0.5
Solder bump height	0.285
Package size	14 × 9

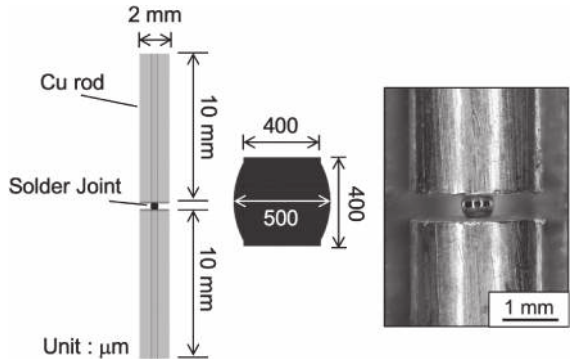

Fig. 3 Geometry and appearance of micro solder joint specimen for the low cycle fatigue test.

bump is shown in Fig. 2 and the dimensions of the package are shown in Table 1.

2.2 Low-cycle fatigue test

The micro solder joint specimen used in this study consisted of two cylindrical copper rods connected by a solder ball of diameter 500 μm (Fig. 3).[7] The cylindrical copper rods had a length of 10 mm and a diameter of 2 mm. The specimen was made such that the shape of the solder joint became the same as the BGA package solder joint, which is described later. Soldering was performed in air with RMA (rosin, mildly activated) flux at 518 K.

A displacement-controlled low-cycle shear fatigue test was conducted. The test temperature was 358 K, which is the

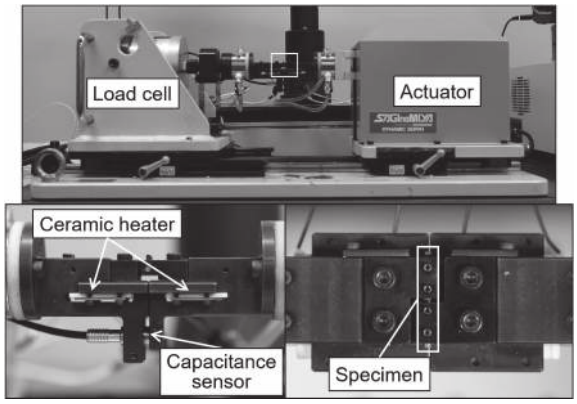

Fig. 4 Appearance of the fatigue testing machine.

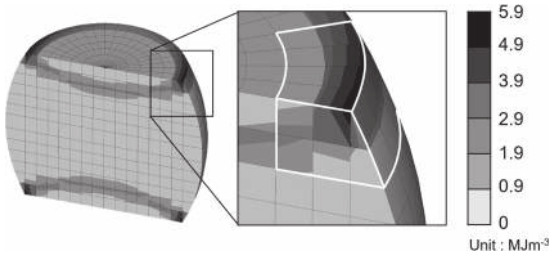

Fig. 5 Contours of inelastic strain energy density in micro solder joint specimen.

highest temperature used in accelerated tests. One of the temperature profiles used for thermal stress analysis of the BGA package is described later. The control wave was a symmetrical triangle waveform. The nominal strain rate was 10^{-3}/s. The fatigue testing machine (LMH207-20: SAGINOMIYA SEISAKUSHO, INC) shown in Fig. 4 was used. This testing machine uses a piezo stage with a displacement-enlarging mechanism as its actuator, with a maximum stroke of ±250 μm and a load cell capacity of ±40 N. The fatigue life was defined as the number of cycles at which the initial load measured during the testing decreased by 50%. The inelastic strain energy density range ΔW_{in} calculated by FEM was used as a parameter for evaluating fatigue life. As an additional note, ΔW_{in} was the volume average of element solutions in the white frame in Fig. 5 equivalent to the crack length at the time when the fatigue life was reached. The calculation formula of ΔW_{in} is given by

$$\Delta W_{in} = \frac{\sum \Delta W_{in}^{element} \cdot V^{element}}{\sum V^{element}} \quad (1)$$

where $\Delta W_{in}{}^{element}$ is the element solution of inelastic strain energy density range, and $V^{element}$ is the volume of the element. The nonlinear kinematic hardening rule (Chaboche model) was used for the strain hardening of solder and the constant was determined from the low cycle fatigue testing by inverse-analysis. Morrow's fatigue life law as shown in eq. (2) was then determined from the relationship between ΔW_{in} calculated by FEM analysis and fatigue life.[8]

$$\Delta W_{in} \cdot N_f^{\beta} = C \quad (2)$$

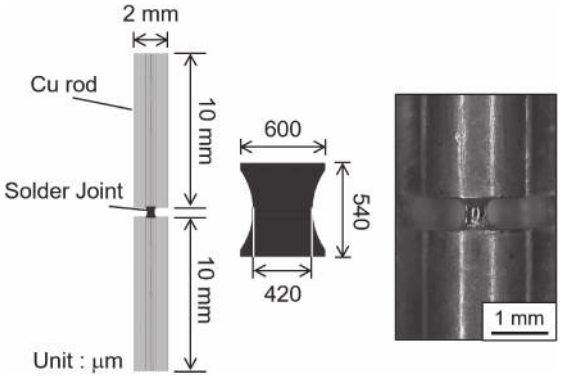

Fig. 6 Geometry and appearance of micro solder joint specimen for creep test.

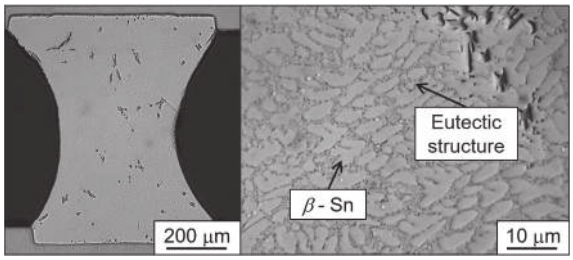

Fig. 7 Optical micrographs of initial microstructure.

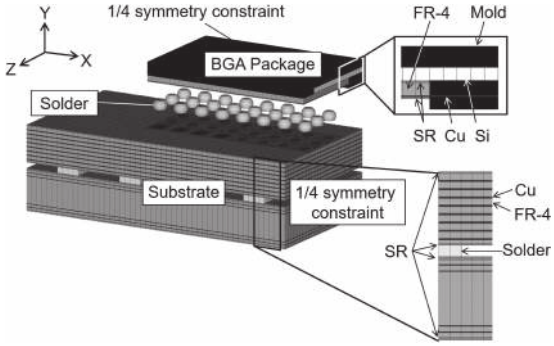

Fig. 8 FEM model of BGA semiconductor package.

Here, ΔW_{in} is the inelastic strain energy density range, N_f is the fatigue life, and β and C are the material constants.

2.3 Stress relaxation test for creep constitutive equation

The creep constitutive equation was determined by the data obtained from stress relaxation testing which was performed at multiple temperatures using a miniature solder joint specimen.[9] The miniature solder joint specimen was created by using two solder balls to join two copper rods. The size of the copper rods was 2 × 10 mm. The soldering conditions were the same as the fatigue test specimen. The specimen and initial microstructure are shown in Figs. 6 and 7. The testing machine was the same as the one used in the low cycle testing. The multi-temperature stress relaxation test procedure was as follows. First, a shear displacement was continuously applied to the specimen at the test temperature of 398 K until steady-state stress appeared. Next, the displacement was held, and the first stress relaxation test was carried out. After the decrease in stress is mostly relieved, the test temperature was set to 348 K and the shear displacement and stress relaxation measurements were again performed. Finally, the temperature was set to 298 K and the third stress relaxation test was performed. Equation (4) was obtained by curve-fitting to the relaxation curve on the assumption that the stress relaxation part of the load-time curve at each temperature would obey Norton's law shown in eq. (3) for the creep at each individual temperature.

$$\dot{\varepsilon} = A\sigma^n \tag{3}$$

$$\frac{1}{\sigma^{n-1}} - \frac{1}{\sigma_i^{n-1}} = (n-1)AEt \tag{4}$$

2.4 Analysis of thermal fatigue of solder joint in BGA packages

Figure 8 shows the FEM model of the BGA package. The FEM model was 1/4 symmetry of the structure in which the BGA package was joined on the FR-4 substrates. The two substrates were connected by solder bumps. The element was a solid 20-node hexahedral and the model scale was 560000 nodes. For the material properties, the solder alloy was treated as an elastic creep body, the mold resin and FR-4 substrates were treated as viscoelastic bodies, and the other constituent materials were treated as elastic bodies. Table 2 shows the material properties of the individual constituent materials. The generalized Maxwell model in eq. (5) was applied to the viscoelastic constitutive equation.

$$E(t) = E_e + \sum_{i=1}^{n} E_i \exp\left(-\frac{t}{\tau_i}\right) \tag{5}$$

where $E(t)$ is the relaxation modulus, E_e is the long-term elastic modulus, n is the Prony series term, E_i and τ_i are

Table 2 Material properties.

	Young's modulus, E / GPa	Poisson's ratio, ν	CTE, α / ppm·K^{-1}
Mold	0.6 ~ 18.8 (Temperature dependent)	0.30	10.0
Si	173	0.35	2.6
SR	2.4	0.29	60
Cu	129.3	0.34	16.6
Solder	76.087-0.109×T [K]	0.30	15
FR-4	8.5 ~ 21.7 (Temperature dependent)	0.28	4.2～15.6

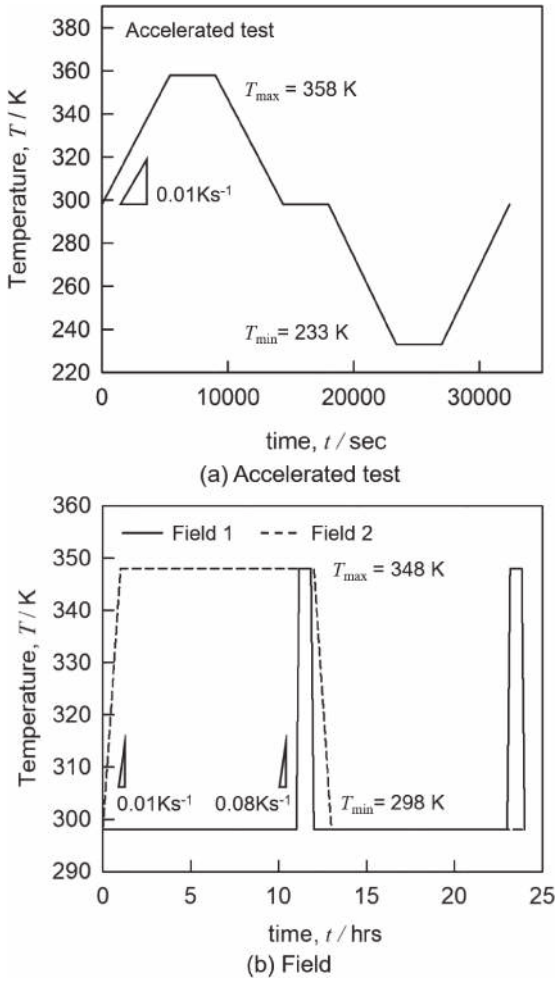

Fig. 9 Profiles of thermal cycling.

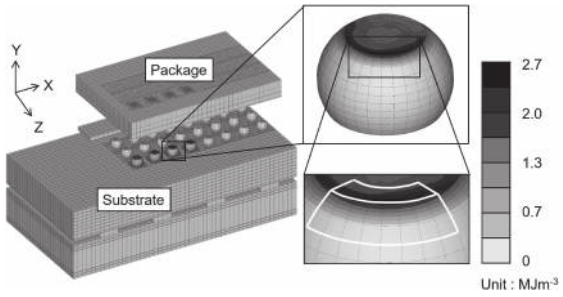

Fig. 10 Contours of inelastic strain energy density in a BGA semiconductor package.

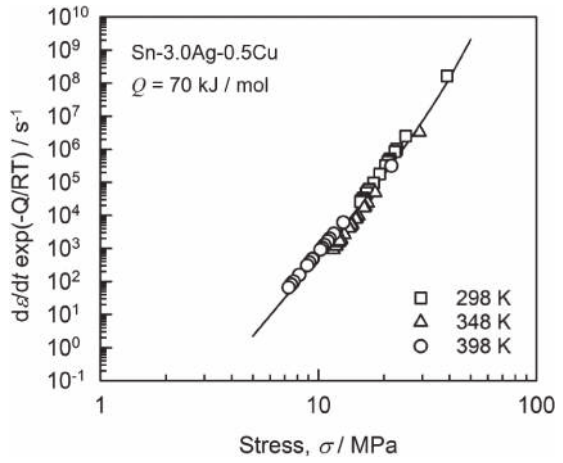

Fig. 11 Relationship between the temperatures compensated strain rate factor and stress.

Prony series approximation coefficients, and t is the relaxation time. Furthermore, fine element meshing was provided to the solder balls at the corners that were most subjected to loads. The temperature cycling conditions used in the FEM analysis were three levels of an accelerated test (233 K ⇆ 358 K) and two temperature profiles to simulate the field environment (298 K ⇆ 348 K). JEITA ET7407-B[10] was used as a reference for the temperature profiles. Figure 9 shows the temperature profiles for each condition. The parameter used for evaluating the thermal fatigue life was the same ΔW_{in} as that in the low cycle fatigue testing and ΔW_{in} per cycle was obtained for the solder bump in which ΔW_{in} was maximum. ΔW_{in} which is obtained from the areas shown in Fig. 10 was the volume average of the element solutions in these areas. Additionally, the element sizes were the same for both the solder bumps in the BGA package and the solder joint in the specimen used in the low cycle fatigue testing. The solver used was a general-purpose code ANSYS ver 18.1.

3. Results and Discussion

3.1 Creep constitutive equation incorporating the microstructural coarsening effect

Figure 11 shows the relationship between the temperature compensated strain rate factor and stress. The relationship between the temperature compensated strain rate factor and the log-log plots of stress became hyperbolic and the generalized Garofalo law in eq. (6) held.

$$\dot{\varepsilon} = A_1[\sinh(\alpha\sigma)]^n \exp\left(-\frac{Q}{RT}\right) \tag{6}$$

where $\dot{\varepsilon}$ is the steady-strain rate, A_1, n, and α are the material constants, Q is the apparent activation energy, R is the gas constant, and T is temperature. A_1, n, α, and Q were 5.75×10^6, 7.8, 0.03, and 70 kJ/mol, respectively. The stress exponent was 7 or more and the strengthening mechanism in Sn–Ag–Cu alloys used in the study was dispersion strengthening by Ag_3Sn.[11–14]

The steady-state creep constitutive equation for metals is commonly represented by the following eq. (7) for all deformation mechanisms.[15,16]

$$\dot{\varepsilon} = \dot{\varepsilon}_0 \frac{G\Omega}{kT}\left(\frac{b}{d_g}\right)^p \left(\frac{\sigma}{G}\right)^n \frac{D}{b^2} \tag{7}$$

where $\dot{\varepsilon}$ is the strain rate, $\dot{\varepsilon}_0$ is the material constant, G is the rigidity, Ω is the atomic volume, k is Boltzmann's constant, T is temperature, b is the Burgers vector, d_g is the crystalline particle diameter, p is the grain diameter exponent, σ is the stress, n is the stress exponent, and D is the diffusion coefficient. In the dislocation creep, the grain diameter exponent p in eq. (7) becomes zero, and the constitutive equation is expressed by eq. (8).

$$\dot{\varepsilon} = \dot{\varepsilon}_0 \frac{G\Omega}{kT}\left(\frac{\sigma}{G}\right)^n \frac{D_{eff}}{b^2} \tag{8}$$

where D_{eff} is the effective diffusion coefficient. The stress exponent is 7 or more in the study, which indicates that the precipitation or dispersion strengthening mechanism is working as a creep deformation mechanism and the creep strength is controlled by the interparticle spacing between dispersoids of Ag_3Sn. Since it is known that dispersoids become coarse by heat diffusion and mechanical strain in long-term use under service conditions,[7] a constitutive equation in which the interparticle spacing is incorporated is required. Equation (8) is regarded as hyperbolic[17] and furthermore when the interparticle spacing is incorporated into the constitutive equation, this gives eq. (9).

$$\dot{\varepsilon} = A_2 \frac{Gb}{kT}\left(\frac{\lambda^2}{d_{\text{p}}}\right)\left[\sinh\left(\frac{\alpha\sigma}{G}\right)\right]^n D_{\text{eff}} \tag{9}$$

where A_2 is the material constant, λ is the interparticle spacing between dispersoids, and d_{p} is the diameter of dispersoid.

$$\frac{\lambda^2}{d_{\text{p}}} = A_3 \frac{r}{V_{\text{f}}^{2/3}} = A_4 r \tag{10}$$

The interparticle spacing λ and the diameter of dispersoid d_{p} in eq. (9) were converted into the particle radius r by using the solid volume ratio V_{f} in eq. (10) to obtain the creep constitutive equation eq. (11) incorporating the growth of dispersoids.

$$\dot{\varepsilon} = A_5 \frac{Gb}{kT} r\left[\sinh\left(\frac{\alpha\sigma}{G}\right)\right]^n D_{\text{eff}} \tag{11}$$

It has been reported in previous studies of Sn–Ag–Cu alloys that an increase in the creep strain rate accompanied by the growth of dispersoids can be expressed by eq. (11).[18–20] Equation (11) was also employed for the creep constitutive equation in the study.

As described above, dispersoids grow due to thermal and strain loads during long-term use. First, the growth of dispersoids is assumed to obey the Lifshitz-Slyozov[21]-Wagner[22] theory of eq. (12).

$$r(t) = Kt^{1/m} \tag{12}$$

where K is the rate constant, t is the time, and m is the growth exponent. Equation (12) represents the growth of dispersoids by thermal diffusion. Since growth of dispersoids in a thermal fatigue environment is caused by thermal and strain, eq. (13) which incorporates strain enhancement into eq. (12) is proposed for the growth of dispersoids.[23,24]

$$r = \left\{\left[K_1 \exp\left(-\frac{Q}{RT}\right)(t + K_2\varepsilon_{\text{in}}N) + r_0^3\right]^{1/m}\right\} \tag{13}$$

where K_1, K_2, and N are constants, Q is the activation energy, R is the gas constant, T is the average temperature of thermal profiles, t is the time, ε_{in} is the inelastic strain, and r_0 is the radius of dispersoids in the initial microstructure. In eq. (13), m represents the growth mechanism, where $m = 2$ when the diffusion mechanism of particle growth is the diffusion of interface between particles and the matrix phase, $m = 3$ for volume diffusion, and $m = 4$ for boundary diffusion.[25] Based on the assumption that particle growth is controlled by volume diffusion, $m = 3$ is used in the study. In the study, t is the total time over which the temperature is above 298 K and T is the integral average of one cycle. K_1, K_2, and Q are determined based on the results of the past study by the author *et al.*[26] The individual constants are shown in Table 3. The relationship between the radii of dispersoids at 348 K and 398 K and the aging times is shown in Fig. 12. The apparent activation energy and K_1 were obtained from the relationship. The activation energy for volume diffusion of Ag in the matrix phase of Sn is approximately 50–70 kJ/mol,[27,28] and the results in Fig. 12 indicate the growth of Ag_3Sn. The relationship between the strain-enhanced growth of Ag_3Sn and cumulative equivalent inelastic strain is shown in Fig. 13. The straight line in Fig. 13 is the result of fitting to eq. (13) and the slope of the line represents the constant K_2. From Fig. 13, K_2 was determined to be 30000. Theoretically, K_1 is given by eq. (14).

$$K_1 = \frac{B\gamma_{\text{s}}V_{\text{m}}CD_0}{RT} \tag{14}$$

Table 3 Material constants of the strain-enhanced model.[26]

K_1	K_2	Q, kJ / mol
6.5×10^{-19}	30000	50

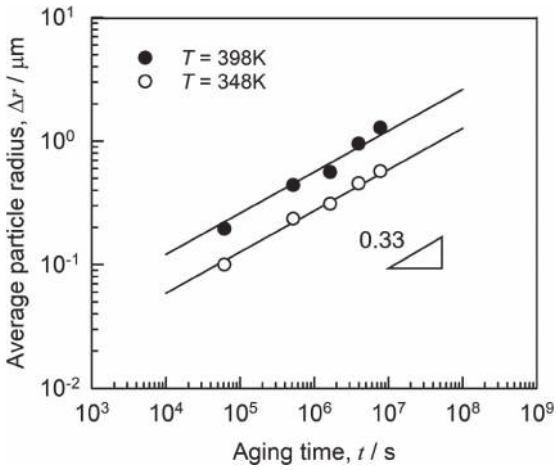

Fig. 12 Relationship between the average particle radius and aging time at each temperature.[26]

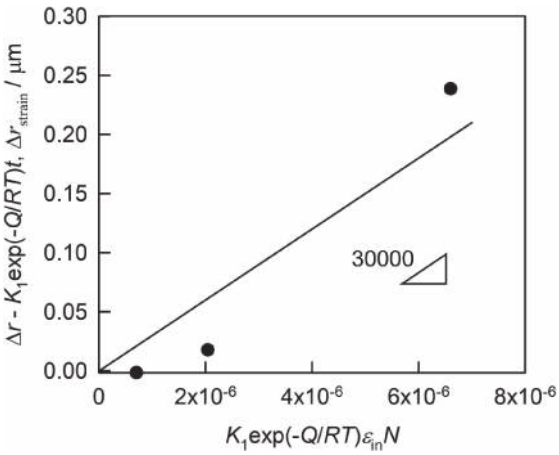

Fig. 13 Strain-enhanced coarsening of intermetallic compounds.[26]

where B is the constant, γ_s is the interface energy between the dispersoids and the matrix phase interfaces, V_m is the molar volume, C is the equilibrium solute concentration, and D_0 is the frequency factor. Although K_1 has temperature dependence associated with the equilibrium concentration and diffusion, K_1 was determined in this study by treating these dependencies as being contained in Q in eq. (13).

The combination of eq. (11) and eq. (13) gives the degradation of creep strength caused by the growth of dispersoid during thermal cycles. In eq. (11), the creep strain rate is proportional to the radius of dispersoid. When the radius of dispersoid grows to r at a given cycle time from r_0 in the initial microstructure, the creep strain rate becomes r/r_0 times. Thus, eq. (15) which is the result of multiplication of the creep constitutive equation obtained from the stress relaxation test by r/r_0 gives the creep constitutive equation at a given cycle time.

$$\dot{\varepsilon} = A_1 \frac{r}{r_0} [\sinh(\alpha\sigma)]^n \exp\left(-\frac{Q}{RT}\right) \tag{15}$$

Individual material constants are the same as in eq. (6). However, the radius of dispersoid r_0 of the specimen for the stress relaxation test is slightly smaller than the radius of dispersoids of the solder joint in the BGA package. Therefore, A_1 which was offset by the ratio of the radius of dispersoid in the stress relaxation test specimen to that in the solder joint of the BGA package is used for the creep constitutive equation of the initial microstructure. The value of r_0 at the time was 0.15 μm and A_1 was 8.63×10^6.

The procedure for performing thermal fatigue analysis of the solder joints in the BGA package is as follows. First, three cycles of temperature cycling were performed by the constitutive equation of the initial microstructure ($r/r_0 = 1$), and then the inelastic strain per cycle in each solder bump (the average of nodal solutions in the area of 60 μm from the top surface of solder bump) was found, and then the creep constitutive equation was updated by the radius r which is calculated at a given cycle by the cycle jump method[29–32] by using eq. (13). The analysis continues using the updated creep constitutive equation to find ΔW_{in} after a given cycle. Thereafter, the creep constitutive equation after a given cycle is updated again and ΔW_{in} is determined. This process is repeated to find the relationship between the number of cycles and ΔW_{in} for the calculation of thermal fatigue life using the damage law obtained by the low cycle fatigue test which is described later. Strictly speaking, the radius r should be calculated by an incremental calculation approach. However, because of difficulty in FEM analysis, r was calculated at each given cycle in this study, for the sake of simplicity.

3.2 Relationship between ΔW_{in} and radius of dispersoids during thermal cycles

Figure 14 shows the relationship between the radius of dispersoid in each temperature profile and the number of cycles. In Fig. 14, the effects of thermal diffusion and strain-enhancement on the growth of the dispersoids are shown separately. The radius of dispersoids increased as the number of cycles increased and the increase in Field 2 was significant. As shown in Fig. 14, the growth of dispersoids

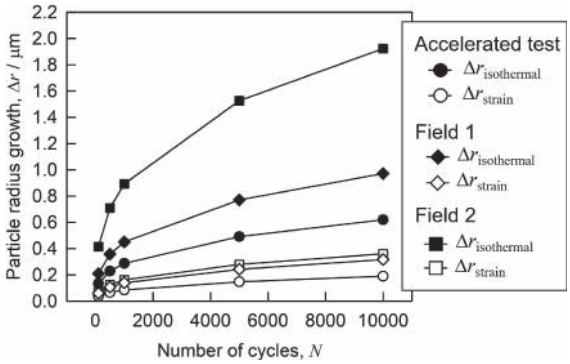

Fig. 14 Relationships between particle radius growth and number of cycles in each profile.

by thermal diffusion was dominant in the study. Since the average temperature in eq. (13) was calculated by the integral average, the average temperature in Field 2 having the longest dwell time was the highest and the growth of dispersions in Field 2 is the largest compared to the other conditions.

Figure 15 shows the relationship between ΔW_{in} in each temperature profile and the number of cycles. As the number of cycles increased, ΔW_{in} increased. This was because the decrease in creep strength accompanied by the growth of dispersoids reduced the deformation resistance of the solder bumps. In particular, the increase in ΔW_{in} during temperature cycling under the field conditions is large, so the effects of microstructural coarsening in the prediction of fatigue life should not be ignored. The relationship between ΔW_{in} shown in Fig. 15 and the number of cycles was described using the power law and its relationship was eq. (16), eq. (17) and eq. (18).

$$\text{Accelerated test} \quad \Delta W_{in} = 0.219 N^{0.0222} \tag{16}$$

$$\text{Field 1} \quad \Delta W_{in} = 0.0463 N^{0.0683} \tag{17}$$

$$\text{Field 2} \quad \Delta W_{in} = 0.0377 N^{0.0666} \tag{18}$$

3.3 Low cycle fatigue life of miniature solder joint specimen

Figure 16 shows the results of the low cycle fatigue test. The vertical axis indicates the inelastic strain energy density range calculated using the FEM analysis and the horizontal axis indicates fatigue life. Morrow's law holds as given by eq. (19).

$$\Delta W_{in} \cdot N_f^{0.8} = 78 \tag{19}$$

where the unit of ΔW_{in} is MJ m^{-3}. The fatigue exponent of the law was 0.8. It has been reported in structural materials that the fatigue exponent approaches 1 at temperatures where creep deformation is dominant.[33] The test temperature in this study was 0.73 T_m, and therefore the fatigue exponent exhibited a value close to 1.

Since ΔW_{in} depends on the number of cycles, the thermal fatigue life of the solder joint in the BGA package was calculated by using the damage law by converting eq. (19) into eq. (20).

$$\int_1^{N_f} \left(\frac{78}{\Delta W_{in}(N)}\right)^{-\frac{1}{0.8}} = 1 \tag{20}$$

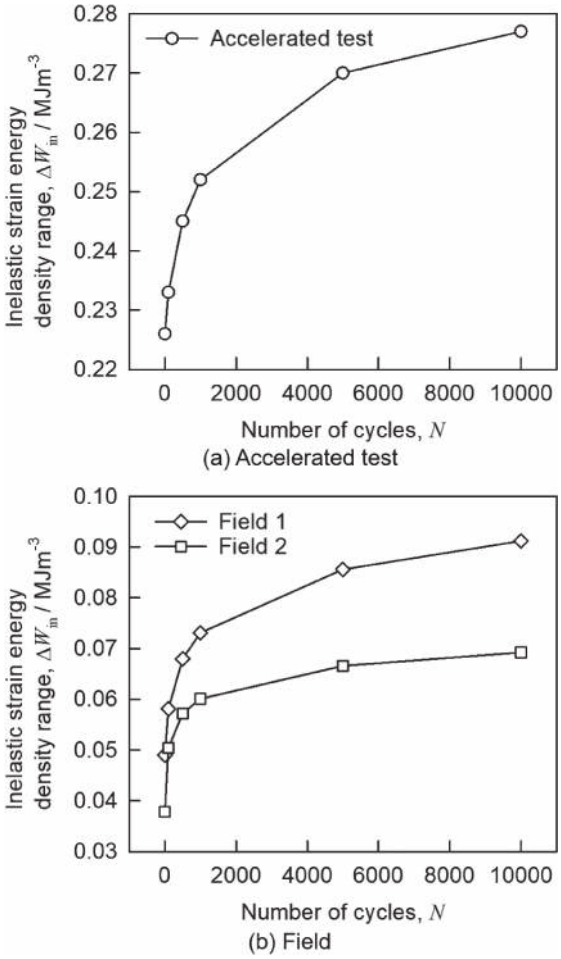

Fig. 15 Relationship between inelastic strain energy density range and number of cycles in each profile.

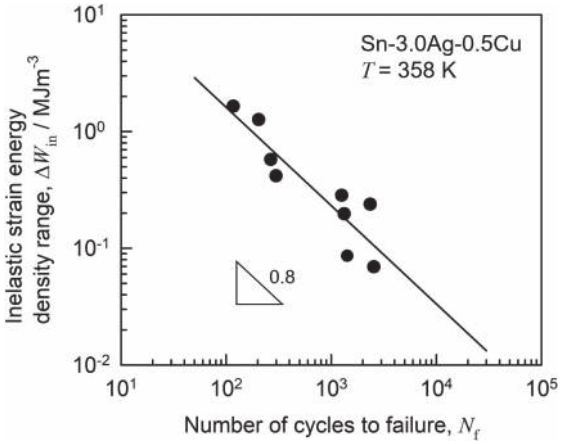

Fig. 16 Relationship between inelastic strain energy density range and number of cycles to failure.

where ΔW_{in} (N) is a function of the cycle dependence of ΔW_{in} as shown in Fig. 15. The number of cycles N_f that satisfy this equation is the thermal fatigue life of the solder joint in the BGA package. It has been reported that Manson-Coffin's law for solder alloys describes the relationship to the dependence on microstructure.[7] For heat resisting steels, it has been reported that the fatigue life is predictable in specimens with different levels of strength processed under

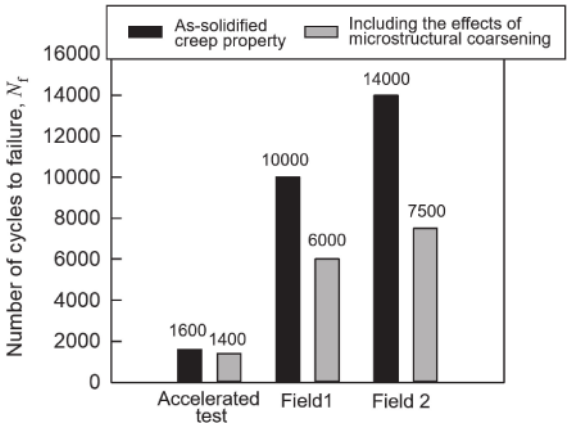

Fig. 17 Predicted thermal fatigue lives in each condition.

different thermal treatments by using Morrow's laws.[34] Since the inelastic strain energy density calculated by integrating stress with strain is used in Morrow's fatigue life laws, the fatigue life is considered insensitive to changes in the strength of the specimen. It was assumed in the study that the fatigue life law of Sn–3.0Ag–0.5Cu alloy was insensitive to microstructural changes.

3.4 Estimation of thermal fatigue life of BGA joint

Figure 17 shows the results of thermal fatigue prediction of the solder joint in the BGA package. Table 3 shows the results of calculating the acceleration factor. The thermal fatigue life calculated by taking into account microstructural coarsening decreased by 13% in the accelerated test, by 40% in Field 1, and by 46% in Field 2 compared to the fatigue life without the microstructural coarsening effect. A major contributor to the decreased strength of Sn–Ag–Cu alloys is thermal diffusion, so the thermal fatigue life under the field conditions with a long dwell time at high temperature is strongly affected by microstructural coarsening. The effects are particularly noticeable in Field 2. However, the decrease in fatigue life caused by microstructural coarsening is small in the accelerated test conditions compared with the field conditions. As Fig. 15 indicates, ΔW_{in} under the accelerated conditions is an order larger than in the field conditions. In the study, when the dependence of ΔW_{in} on the number of cycles was substituted into eq. (20), the number of cycles at which the integral value reaches one is the thermal fatigue life. In the accelerated test with a large ΔW_{in}, the number of cycles that satisfy eq. (20) is very short compared with that in the field and the life cycle is attained before the coarsening effects appear. This means that under loading conditions where ΔW_{in} is large and the fatigue life is short, the decrease in the fatigue life due to microstructural changes is small. This affects the calculation of acceleration factors. When the microstructural coarsening effect was taken into account, the acceleration factors decreased by about 32% in Field 1 and about 39% in Field 2 as shown in Table 4.

4. Conclusions

A method of predicting thermal fatigue life of solder joints in BGA packages was proposed that focuses on the decrease

Table 4 Acceleration factor under field conditions.

	Acceleration factor	
	Field 1	Field 2
As-solidified creep property	6.2	8.7
Including the effects of microstructural coarsening	4.2	5.3

in creep strength caused by microstructural coarsening that occurs during the use of the packages. The findings were as follow.

(1) In the solder alloy of Sn–Ag–Cu, the dispersoid (Ag_3Sn) size increases as the number of thermal cycles increases, and the resistance to creep deformation of the solder bump decreases at the same time. The decrease in resistance to creep deformation causes an increase in the inelastic strain energy density range ΔW_{in} which is the driving force of fatigue fracture in solder.

(2) In this study, the growth of dispersoid caused by thermal diffusion was dominant compared to that by strain-enhanced effect. Therefore, the growth was large in temperature profiles with high average temperatures and long dwell times.

(3) The thermal fatigue life calculated using the creep constitutive equation incorporating the microstructural coarsening effect decreased compared to that calculated without the microstructural coarsening effect, by 13% in the accelerated test, 40% in Field 1, and 46% in Field 2. Under loading conditions with large ΔW_{in} and short fatigue life, the decrease in fatigue life caused by the microstructural coarsening effect was small.

(4) The acceleration factor including the effect of microstructural coarsening decreased by about 32% in Field 1 and 39% in Field 2.

REFERENCES

1) W.W. Lee, L.T. Nguyen and G.S. Selvaduray: Microelectron. Reliab. **40** (2000) 231–244.
2) S. Su, F.J. Akkara, R. Thaper, A. Alkhazali, M. Hamasha and S. Hamasha: J. Electron. Packag. **141** (2019) 040802.
3) L. Qi, J. Huang, X. Zhao and H. Zhang: J. Alloy. Compd. **469** (2009) 102–107.
4) L. Yin, L. Wentlent, L. Yang, B. Arfaei, A. Oasaimeh and P. Borgesen: J. Electron. Mater. **41** (2012) 241–252.
5) H. Ma and J.C. Suhling: J. Mater. Sci. **44** (2009) 1141–1158.
6) J. Zhang, Z. Hai, S. Thirugnanasambandam, J.L. Evans, M.J. Bozack, Y. Zhang and J.C. Suhling: IEEE Trans. Compon., Packag. Manufact. Technol. **3** (2003) 1348–1357.
7) Y. Kanda, Y. Kariya and Y. Oto: J. Electron. Mater. **41** (2012) 580–587.
8) J.D. Morrow: *Cyclic Plastic Strain Energy and Fatigue od Metals*, (ASTM Spec. Tech Publ., 378, 1964) pp. 45–87.
9) Y. Kanda and Y. Kariya: Microelectron. Reliab. **52** (2012) 1435–1440.
10) Japan Electronics and Information Technology Industries Association: JEITA Standard. ET-7407B (2012) 9–13.
11) Y. Kariya, M. Otsuka and W.J. Plumbridge: J. Electron. Mater. **32** (2003) 1398–1402.
12) W. Yang, L.E. Felton and R.W. Messler: J. Electron. Mater. **24** (1995) 1465–1472.
13) M.M. EL-Bahay, M.E. EL Mossalamy, M. Mahdy and A.A. Bahgat: J. Mater. Sci. **15** (2004) 519–526.
14) Y. Kariya, T. Asai, T. Suga and M. Otsuka: TMS Letter **1** (2004) 169–170.
15) A.K. Mukherjee, J.E. Bird and J.E. Dorn: *The Interaction between Dislocations and Point Defects*, ed. by B.L. Eyre, (United Kingdom Atomic Energy Authority, Harwell, UK, 1968) pp. 422–495.
16) A.K. Mukherjee, J.E. Bird and J.E. Dorn: Trans. Am. Soc. Met. **62** (1969) 155–179.
17) F. Garofalo: Trans. Metall. AIME **227** (1963) 351–356.
18) I. Dutta, P. Kumar and G. Subbarayan: JOM **61** (2009) 29–38.
19) M. Hasnine, M. Mustafa, J.C. Suhling, B.C. Prorok, M.J. Bozack and P. Lall: Proc. 63rd IEEE Electronic Components & Technology Conference, (2013) pp. 166–178.
20) S. Wiese and K.J. Wolter: Microelectron. Reliab. **47** (2007) 223–232.
21) I. Dutta: J. Electron. Mater. **32** (2003) 201–207.
22) I.M. Lifshitz and V.V. Slyozov: J. Phys. Chem. Solids **19** (1961) 35–50.
23) C. Wargner: Z. Electrochem. **65** (1961) 581.
24) I. Dutta, D. Pan, R.A. Marks and S.G. Jadhav: Mater. Sci. Eng. A **410–411** (2005) 48–52.
25) S.L. Allen, M.R. Notis, R.R. Chromik and R.P. Vinci: J. Mater. Res. **19** (2004) 1417–1424.
26) Y. Kanda, Y. Kariya and T. Tasaka: Mater. Trans. **53** (2012) 2072–2077.
27) R.W. Wu, L.C. Tsao, S.Y. Chang, C.C. Jain and R.S. Chen: J. Mater. Sci. Mater. Electron. **22** (2011) 1181–1187.
28) F. Vnuk, M.H. Ainsley and R.W. Smith: J. Mater. Sci. **16** (1981) 1171–1176.
29) K. Satoh, Y. Yusa and H. Okada: Trans. JSME **83** (2017) (in Japanese).
30) K. Satoh, Y. Yusa and H. Okada: Trans. JSME **85** (2019) (in Japanese).
31) D. Cojocaru and A.M. Karlsson: Int. J. Fract. **28** (2006) 1677–1689.
32) W.V. Paepegem, J. Degrieck and P.D. Baets, Compos. B. Eng. **32** (2001) 575–588.
33) R. Otani: Introduction to Fracture Mechanics **10** (1984) 609–615 (in Japanese).
34) D.M. Li, K.W. Kim and C.S. Lee: Int. J. Fatigue **19** (1997) 607–612.